BIOCHEMISTRY

 Volume 44, Number 17 May 3, 2005

Current Topics

Structural and Catalytic Diversity within the Amidohydrolase Superfamily†

Clara M. Seibert and Frank M. Raushel*

Department of Chemistry, P.O. Box 30012, Texas A&M University, College Station, Texas 77842-3012

Received December 20, 2004; Revised Manuscript Received March 16, 2005

ABSTRACT: The amidohydrolase superfamily comprises a remarkable set of enzymes that catalyze the hydrolysis of a wide range of substrates bearing amide or ester functional groups at carbon and phosphorus centers. The most salient structural landmark for this family of hydrolytic enzymes is a mononuclear or binuclear metal center embedded within the confines of a $(\beta/\alpha)_8$-barrel structural fold. Seven variations in the identity of the specific amino acids that function as the direct metal ligands have been structurally characterized by X-ray crystallography. The metal center in this enzyme superfamily has a dual functionality in the expression of the overall catalytic activity. The scissile bond of the substrate must be activated for bond cleavage, and the hydrolytic water molecule must be deprotonated for nucleophilic attack. In all cases, the nucleophilic water molecule is activated through complexation with a mononuclear or binuclear metal center. In the binuclear metal centers, the carbonyl and phosphoryl groups of the substrates are polarized through Lewis acid catalysis via complexation with the β-metal ion, while the hydrolytic water molecule is activated for nucleophilic attack by interaction with the α-metal ion. In the mononuclear metal centers, the substrate is activated by proton transfer from the active site, and the water is activated by metal ligation and general base catalysis. The substrate diversity is dictated by the conformational restrictions imposed by the eight loops that extend from the ends of the eight β-strands.

A comprehensive understanding of the intimate relationship between protein structure and enzymatic activity is an unsolved problem that is essential for deciphering substrate specificity for proteins of unknown function and the creation of novel catalytic activities from existing active site templates. The amidohydrolase superfamily of enzymes is a well-documented example for the divergence of protein architecture and the associated catalytic transformations that can arise from a common ancestral precursor. Holm and Sander first identified the amidohydrolase superfamily from the three-dimensional structural similarities within the active sites and global protein folds of urease (URE),[1] phosphotriesterase (PTE), and adenosine deaminase (ADA) (*1*). The most salient structural landmark for this family of predominantly hydrolytic enzymes is a mononuclear or binuclear metal center embedded within the confines of a protein possessing a $(\beta/\alpha)_8$-barrel structural fold. The metal center in this enzyme superfamily has a dual functionality in the expression of the overall catalytic activity. The scissile bond of the substrate must be activated for bond cleavage, and the hydrolytic water molecule must be enhanced for nucleophilic attack. Since

† This work was supported in part by the NIH: GM 33894 and GM 71790.

* To whom correspondence should be addressed: e-mail: raushel@tamu.edu; fax: (979) 845-9452; phone: (979) 845-3373.

[1] Abreviations: PTE, phosphotriesterase; ADA, adenosine deaminase; CDA, cytosine deaminase; AGD, acetyl glucosamine-6-phosphate deacetylase; URE, urease; PHP, phosphotriesterase homology protein; DHO, dihydroorotase; IAD, isoaspartyl dipeptidase; D-HYD, D-hydantoinase; L-HYD, L-hydantoinase; RDP, renal dipeptidase; URI, uronate isomerase; DAA, D-amino acid deacetylase.

10.1021/bi047326v CCC: $30.25
Published on Web 04/09/2005

the initial discovery of the amidohydrolase superfamily in 1997, the number of documented members within this enzyme group now exceeds 1000.

There are currently 16 unique members of the amidohydrolase superfamily for which high-resolution X-ray crystal structures are available.[2] The detailed protein structures, coupled in some cases with an elucidation of the catalytic reaction mechanisms, have significantly enhanced our knowledge of the range of catalytic and structural diversity within this enzyme superfamily. This group of enzymes catalyzes reactions involving amino acids, sugars, nucleic acids, and organophosphate esters. In this assessment of the amidohydrolase superfamily, the structural and mechanistic diversity within the active site will be described and correlated with the subsequent evolution of the reaction and substrate specificity.

CHEMICAL REACTIONS

Of the 16 nonredundant protein structures that have been deposited in the Protein Data Bank (PDB) for members of the amidohydrolase superfamily, there are three enzymes for which the chemical reactions have not, as yet, been characterized. One of these enzymes, the PTE homology protein (PHP) from *Escherichia coli*, is most structurally similar to PTE, but it does not catalyze the hydrolysis of organophosphate triesters (*2*). The catalytic reactions for two other proteins from *Thermotoga maritima*, solved by the efforts of the Joint Center for Structural Genomics, also have not been identified. However, based on current sequence alignments, the protein Tm0667 (PDB entry 1j6o) may function to hydrolyze nucleic acids, while protein Tm0936 (PDB entry 1j6p) likely catalyzes a hydrolytic substitution within a heteroaromatic base. The remaining structurally characterized members of the amidohydrolase superfamily catalyze hydrolytic reactions with the single exception of uronate isomerase (URI), which catalyzes an aldose/ketose isomerization reaction between D-glucuronate and D-fructuronate (*3*). PTE catalyzes the hydrolysis of a phosphorus−oxygen bond within an organophosphate triester (*4*, *5*). The rest of the structurally characterized proteins catalyze the cleavage of C−N bonds. Seven of these examples catalyze the hydrolysis of amide bonds: urease (URE) (*6*, *7*), dihydroorotase (DHO) (*8*), iso-aspartyl dipeptidase (IAD) (*9*), the various hydantoinases, D-HYD (*10*, *11*) and L-HYD (*12*), renal dipeptidase (RDP) (*13*), *N*-acetyl glucosamine-6-phosphate deacetylase (AGD) (*14*) and D-amino acid deacetylase (DAA) (*15*). Two other proteins, adenosine deaminase (ADA) (*16*) and cytosine deaminase (CDA) (*17*), catalyze the elimination of ammonia from aromatic bases. There are three separate entries for HYD that catalyze the cleavage of hydantoins with alternative stereochemical and structural constraints. The chemical diversity for substrates recognized by the amidohydrolase superfamily is illustrated in Scheme 1.

Scheme 1

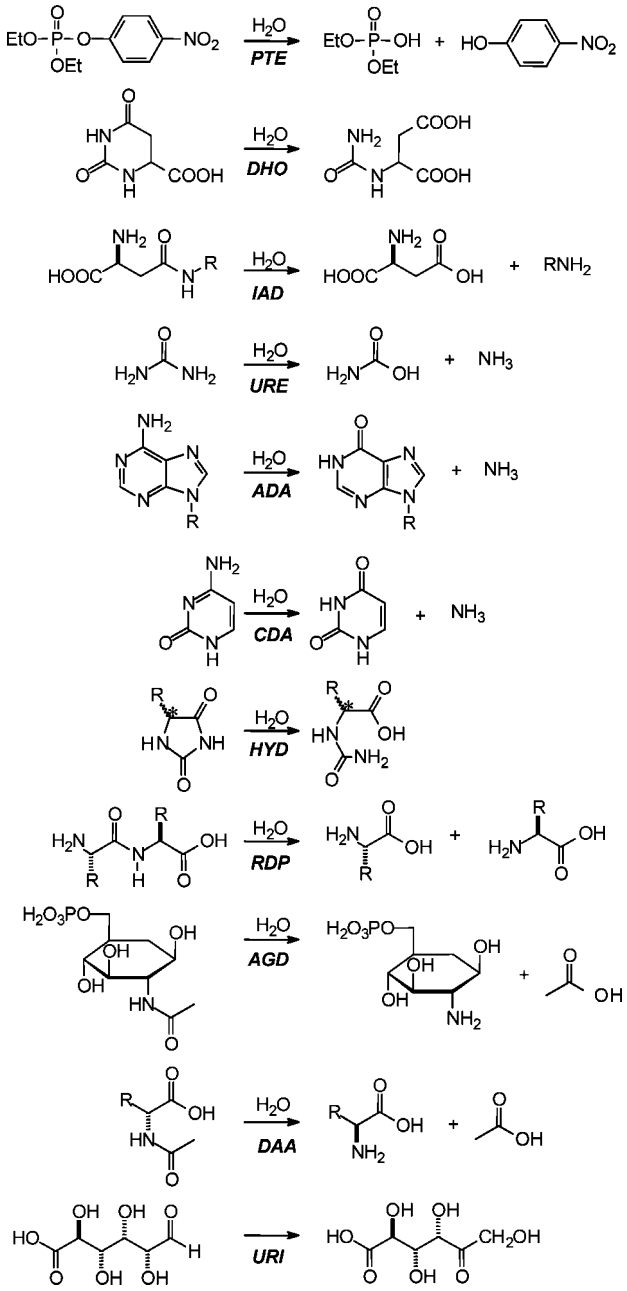

DIVALENT METAL CENTER

There are seven structurally characterized variations of the divalent metal centers within the amidohydrolase superfamily (Table 1). The prototypical and most common metal center, subtype I, is the form of the binuclear metal center found in PTE, DHO, IAD, URE, and the three versions of HYD. In all seven proteins, the two divalent cations are separated by approximately 3.6 Å and are ligated to the protein through electrostatic interactions with the side chains of six amino acids. The more buried metal ion, M_α, is coordinated to two histidine residues from strand 1 of the β-barrel and an aspartate from strand 8. The more solvent-exposed metal ion, M_β, is ligated to two imidazole side chains of histidine from strands 5 and 6. The two divalent cations are bridged by a hydroxide in addition to a carbamate functional group that originates from the posttranslational modification of a lysine

[2] Protein Data Bank structures referenced: PHP, 1bf6 (*2*); URI, 1j5s (*3*); PTE: 1hzy (*4*) and 1ez2 (*5*); URE, 2ubp (*6*) and 2kau (*7*); DHO: 1j79 (*8*); IAD, 1onw and 1onx (*9*); D-HYD, 1gkp (*10*) and 1k1d (*11*); L-HYD, 1gkr (*12*), RDP: 1itq and 1itu (*13*); AGD, 1o12 and 1un7 (*14*), DAA: 1m7j (*15*); ADA: 1a4m (*16*), CDA, 1k6w and 1k70 (*17*); tatD-related deoxyribonuclease, 1j6o; metal-dependent hydrolase of cytosine deaminase/chlorohydrolase family, 1j6p.

Table 1: Variations of the Metal Ligands to the Mononuclear and Binuclear Metal Centers in the Amidohydrolase Superfamily

			strand							
subtype	metals	positions	1	2	3	4	5	6	7	8
I	Zn, Ni	α, *β*	HxH			K	H	H		D
II	Zn	α, *β*	HxH			E	H	H		D
III	Zn, Fe	α	HxH				H	h[b]		D
IV	Fe	*β*	hxh[a]		E		H	H		d[b]
V	Zn	*β*	hxh[a]	C			H	H		d[b]
VI	Zn	α, *β*	HxD		E		H	H		d[b]
VII			HxH				H			D

[a] These residues are in the active site but do not appear to be ligated directly to the divalent cation. The specific function of these residues is uncertain and in some cases a second metal can be accommodated in the site, but the second metal ion is apparently not required for catalytic activity. [b] These residues are not ligated directly to one of two divalent cations but are hydrogen bonded to the hydrolytic water molecule.

residue from strand 4. The binuclear metal centers can self-assemble in the presence of bicarbonate (*18*), but it is uncertain whether there are other accessory proteins that catalyze the assembly process in the cell other than with urease (*19*).

Virtually the same structural motif is observed in subtype II except the carboxylated lysine residue is replaced with a glutamate from strand 4. The only member of this particular subtype for which there is a structure is the PTE homology protein (PHP) from *E. coli*. In PHP, an alanine residue has been inserted into the amino acid sequence immediately prior to the bridging glutamate residue. This insertion functions to push the glutamate forward, so the side chain carboxylate can occupy the same relative position as the carbamate group from the carboxylated lysine of the PTE subgroup. Representations of these two binuclear metal centers are found in Figure 1A,B.

The divalent cation centers of subtype III, found in adenosine deaminase and cytosine deaminase, have only a single metal ion in the active site. In these two proteins, the lone metal ion occupies the same physical location as M_α in the PTE subgroup, and the side chain ligand from *β*-strand 4 that would normally bridge the two metal ions is missing. The conserved histidine residue from strand 5 is rotated into the space normally occupied by the bridging side chain of subtypes I and II and is ligated directly to M_α. The conserved histidine residue from strand 6 is not ligated to any metal ion but appears to function in catalysis as a general base during proton abstraction from the water molecule that is directly coordinated to the single metal ion at position M_α. It is curious to note that while ADA and CDA catalyze very similar chemical reactions, ADA is a Zn-dependent enzyme (*20*), while CDA apparently requires ferrous iron for catalytic activity (*21*). A representative example of this type of metal center is shown in Figure 1C.

Subtype IV is exemplified by AGD (*T. maritima*) which, like CDA, has a mononuclear iron center embedded within the active site. However, the metal ion occupies the M_β site rather than the M_α site. The iron is directly coordinated to the side chains from three amino acids originating from the *β*-barrel. Two of these side chains are from the histidines in strands 5 and 6. The third protein ligand is an uncommon glutamate from strand 3 rather than strand 4. Also bound to this metal ion are two water molecules. One of these water molecules is further hydrogen bonded to the invariant aspartate residue from strand 8 and the second histidine from strand 1. The AGD from *T. maritima* has all of the metal ligands found in the PTE subgroup except for the bridging carboxylate from strand 4. From the X-ray crystal structure, it appears that the two histidines from strand 1 do not contribute to metal binding. In addition, Glu-115 from strand 3 appears to be positioned as a potential bridging carboxylate. This suggests that the *T. maritima* enzyme may be able to bind two metal ions under the proper conditions. This conclusion is supported by the observation that the AGD homologue from *B. subtilis* also has a bridging carboxylate from strand 3 and does have two metals in the X-ray crystal structure (*14*). However, in the AGD homologue from *E. coli*, the two conserved histidine residues from strand 1 have been replaced with glutamine and asparagine (gi: 16128653), residues that are not commonly found to ligate metals, suggesting that the enzyme can indeed function with only a single metal ion at the M_β site. The ligation geometry for the AGD metal center from *T. maritima* is presented in Figure 1D.

The metal center within the active site of the other deacetylase, DAA, is from subtype V and also functions with a single divalent cation at the M_β-position. An additional metal ion can be forced into the active site at high concentrations (*15*, *22*). However, the second metal ion is not critical for catalytic activity. Like *E. coli* AGD, this active site contains all of the protein ligands found in the PTE subgroup, except the bridging carboxylate from strand 4. The tightly bound metal ion is ligated to the two histidines from strands 5 and 6 in addition to a cysteine from strand 2. Thus far, this is the only structurally characterized example from this superfamily that utilizes a cysteine as a direct metal ligand and the only protein that uses a structural or catalytic residue from strand 2. The aspartate from strand 8 is poised to serve as an acid/base catalyst in activation of the hydrolytic water molecule. The structure of the divalent cation site in DAA is illustrated in Figure 1E.

The renal dipeptidase from humans is apparently the most distantly related member of the amidohydrolase superfamily for which there is a three-dimensional structure (*13*). There are two particularly interesting aspects of the renal dipeptidase structure. The protein binds 2 equiv of zinc, but the bridging ligand is a glutamate rather than a carboxylated lysine residue and originates from strand 3 rather than from strand 4. This feature is reminiscent of what is observed in subtype IV with AGD. In addition, the second histidine residue from the HxH motif within strand 1 is substituted with an aspartic acid residue. In this structure one of the *δ* oxygens from the aspartic acid replaces the *ϵ*2 nitrogen of the second histidine. The other *δ* oxygen apparently replaces the coordination function of the aspartate that usually coordinates M_α from strand 8. The highly conserved aspartate from strand 8 is present; however, its function, as deduced from the X-ray structure, appears to be formation of a hydrogen bond with the hydrolytic water rather than to ligate M_α. In addition to these residues, there is a histidine from strand 4 that has been proposed to function in the stabilization of the tetrahedral intermediate. It thus appears that the catalytic reaction mechanism of the renal dipeptidase may be somewhat different from the proposed chemical mechanisms of the other amidohydrolases. The structure of the

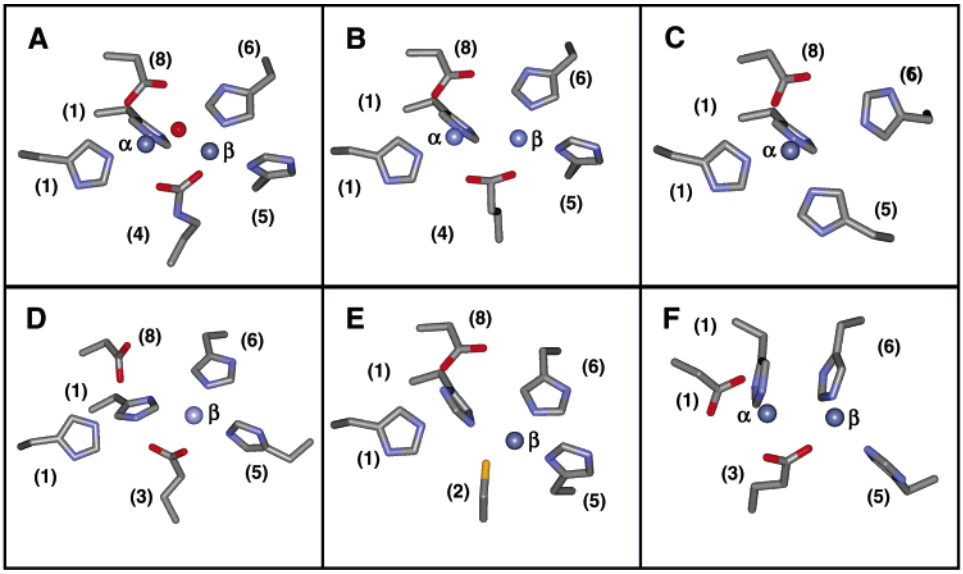

FIGURE 1: Comparison of six variations for the binding of one or two divalent cations to the active site of enzymes within the amidohydrolase superfamily. (A) Subtype I (PTE, from PDB file: 1hzy); (B) subtype II (PHP, from PDB file: 1bf6); (C) subtype III (ADA, from PDB file: 1a4m); (D) subtype IV (AGD, from PDB file: 1o12); (E) subtype V (DAA, from PDB file: 1m7j); (F) subtype VI (RDP, from PDB file: 1itq). The ligands are annotated according to the specific strand within the β-barrel from which they originate. The metal ions are depicted as blue spheres. The figures were drawn using WebLab Viewer Pro.

divalent metal center in the renal dipeptidase is illustrated in Figure 1F.

The final variant of divalent cation centers, subtype VII, is represented by uronate isomerase (URI) and is not fully characterized (*3*). The initial structure was solved in the absence of added metal ions, although there is density consistent with either a metal ion or a water molecule in the active site. It is known from a comparison of the holo- and apo-enzymes within this family of enzymes that there can be large structural changes in the active site in the absence of divalent cations, which can make it difficult to identify the residues that directly coordinate the metals (*23*). Nevertheless, structural alignments demonstrate that URI has the commonly conserved HxH motif from strand 1, a histidine from strand 5, and an aspartate from strand 8. This is the only structurally characterized amidohydrolase member that does not have a histidine at the end of strand 6. However, there are a number of amino acid residues that are found at the ends of the remaining strands that could function as either direct metal ligands or catalytic side chains.

A superposition of the six subtypes of structurally characterized divalent cation centers is presented in Figure 2. This figure graphically illustrates the apparent plasticity of the protein architecture for changes in the number of bound divalent cations and the introduction of direct metal ligands or acid/base catalysts from nearly every strand within the $(\beta/\alpha)_8$-barrel. A majority of the systems identified thus far operate as binuclear metal centers, but it is clear that simpler variations have evolved that function quite well with a single divalent cation. For proteins that bind two divalent cations the bridging protein ligand is predominantly a posttranslationally modified lysine residue from strand 4 or less often a glutamate from strand 3 or 4. Direct metal ligands are contributed by the side chains of aspartate, glutamate, histidine, and cysteine. The histidine residue from strand 5 is, however, the only metal ligand that has been retained in all of the structurally characterized metal centers. The conservation in the position of the atoms that directly ligate the metal ions

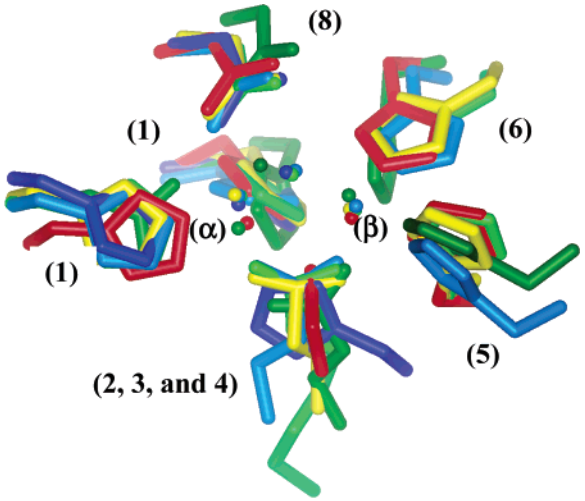

FIGURE 2: Overlay of the metal center for selected members of the amidohydrolase superfamily. The individual metal centers are color coded according to the following format: PTE, from PDB file: 1hzy (light green); PHP, from PDB file: 1bf6 (yellow); ADA, from PDB file: 1a4m (dark blue); AGD, from PDB file: 1o12 (light blue); DAA, from PDB file: 1m7j (red); and RDP, from PDB file: 1itq (dark green).

is noteworthy. The RMS deviation for these atoms span from 0.2 to 0.6 Å between pairs of structures, despite the numerous substitutions and sequence rearrangements.

SECONDARY METAL LIGANDS

The secondary metal ligands, those residues that hydrogen bond or ion pair with the direct metal ligands, are quite variable among those members of the amidohydrolase superfamily for which crystal structures are available. This is particularly true for the multiple examples that possess the binuclear metal center of subtype I. For example, His-254 from the end of strand 7 in PTE hydrogen bonds with the direct metal ligand, Asp-301 from strand 8 (*4*). None of the other structures of subtype I show this interaction, but

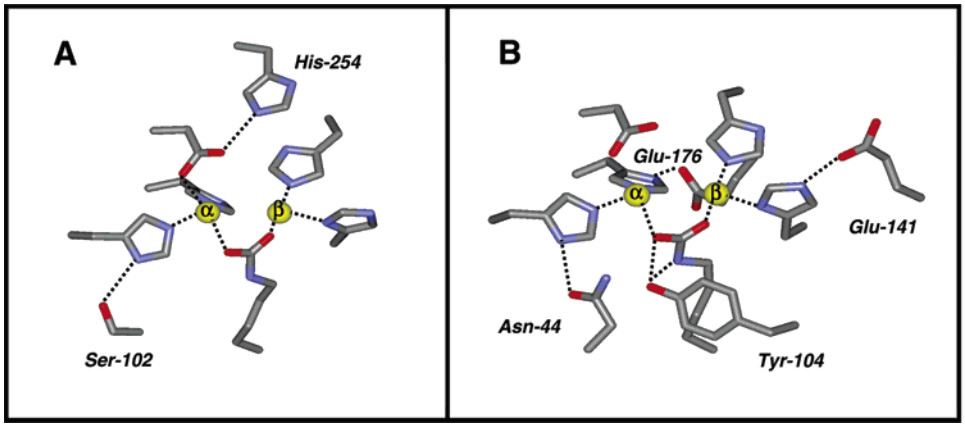

FIGURE 3: Primary and secondary metal ligands in PTE (A) and DHO (B). In PTE His-254 is hydrogen bonded with Asp-301 from strand 8, and Ser-102 is hydrogen bonded to His-57 from strand 1 (taken from PDB file: 1hzy). In DHO Asn-44 is hydrogen bonded to His-18 from strand 1, and Tyr-104 is hydrogen bonded to the carboxylated Lys-102 from strand 4. Glu-141 and Glu-176 are hydrogen bonded to His-139 and His-16, respectively (taken from PDB file: 1j79).

this cluster of amino acids has been proposed to facilitate the shuttling of protons away from the active site of PTE during substrate turnover (*24*). The second histidine within the HxH motif from PTE interacts with Ser-102, which is positioned just after the end of strand 2. PHP, DHO, and RDP have similar contacts with other residues found in the loop that follows strand 2, while the other structurally characterized members of the amidohydrolase superfamily do not exhibit such interactions. The aspartic acid in the HxD motif from strand 1 of RDP has an additional interaction with the invariant aspartic acid from strand 8. The highly conserved aspartic acid residue from strand 8 is usually a direct metal ligand to M_α in all of the other structures, but in RDP this aspartic acid hydrogen bonds only with the bridging hydroxide (*13*).

The carboxylated lysine of PTE does not hydrogen bond with any other residues. However, in some of the other structures the residues that bridge the two divalent cations also interact with the side chains of other amino acids within the active site. For example, in DHO the carboxylated Lys-102 is hydrogen bonded to Tyr-104 (*8*) but in URE the carboxylated lysine is hydrogen bonded to Thr-172 (*6*). The histidine from strand 5 has no other contacts in PTE. However, the homologous residues in PHP, DHO, and all three of the hydantoinases make contact with a serine or glutamate residue that is two residue positions removed from the direct metal ligand from the same β-strand. The conserved histidine from strand 5 has other, less conserved, contacts in URE, ADA, and RDP. The histidine from strand 6 of PTE interacts with no other amino acids in the active site other than with M_β. However, in ADA this residue interacts with Tyr-240 from strand 6. In PHP and DAA, the conserved histidine from strand 6 interacts with Asp-209 at the end of strand 7 and Glu-224 from loop 5. The highly conserved aspartic acid from strand 8 has no interactions beyond the first histidine of the HxH motif and the catalytic hydroxide. The specific functions of these secondary interactions in the structure and function of the amidohydrolase superfamily have not, as yet, been ascertained via the characterization of mutant enzymes. The significant variability of the secondary metal ligands suggests that the primary role of these interactions is in the structural maintenance of the active site rather than modulation of the electrostatic environment for the metal center. A comparison of the secondary metal interactions in DHO and PTE is presented in Figure 3.

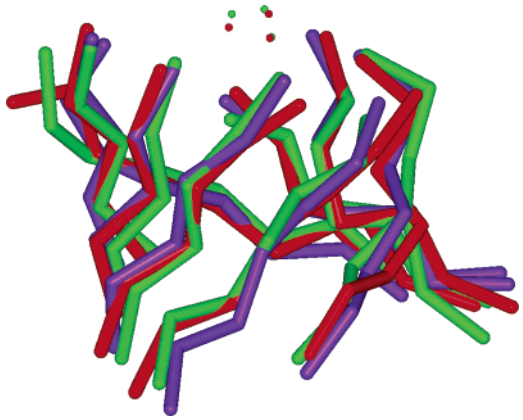

FIGURE 4: Overlay of the eight β-strands for PTE, from PDB file: 1hzy (bright green); DHO, from PDB file: 1j79 (red); and IAD, from PDB file: 1onw (purple).

BETA BARREL

The β-barrel core within the amidohydrolase superfamily is formed from the interaction of 8 β-strands in a manner similar to other proteins previously identified as $(\beta\alpha)_8$-barrel proteins (*1*). The main chain atoms of these eight strands overlay very well among the structures of the amidohydrolase superfamily members determined thus far. A superposition of the Cα atoms for the β-barrels gives an RMSD $= 1.5 \pm 0.3$ Å. Occasionally there is a deletion or insertion in a strand that causes a single residue interruption of the secondary structure. On the C-terminal side of the β-barrel the metal binding residues that form the core of the mononuclear and binuclear metal centers deviate somewhat from one another. The structural overlay presented in Figure 4 was constructed by aligning the β-strands only. There is scant sequence conservation in the β-strands prior to the metal binding residues with the single exception of the amino acid that is two residue positions before the first histidine in the HxH motif from strand 1. This residue is often an aspartate or glutamate and anchors the backbone of the first histidine. However, PTE and PHP do not have this structural feature. It is interesting to note that the metal ligands and the α-helices superimpose remarkably well when the β-strands

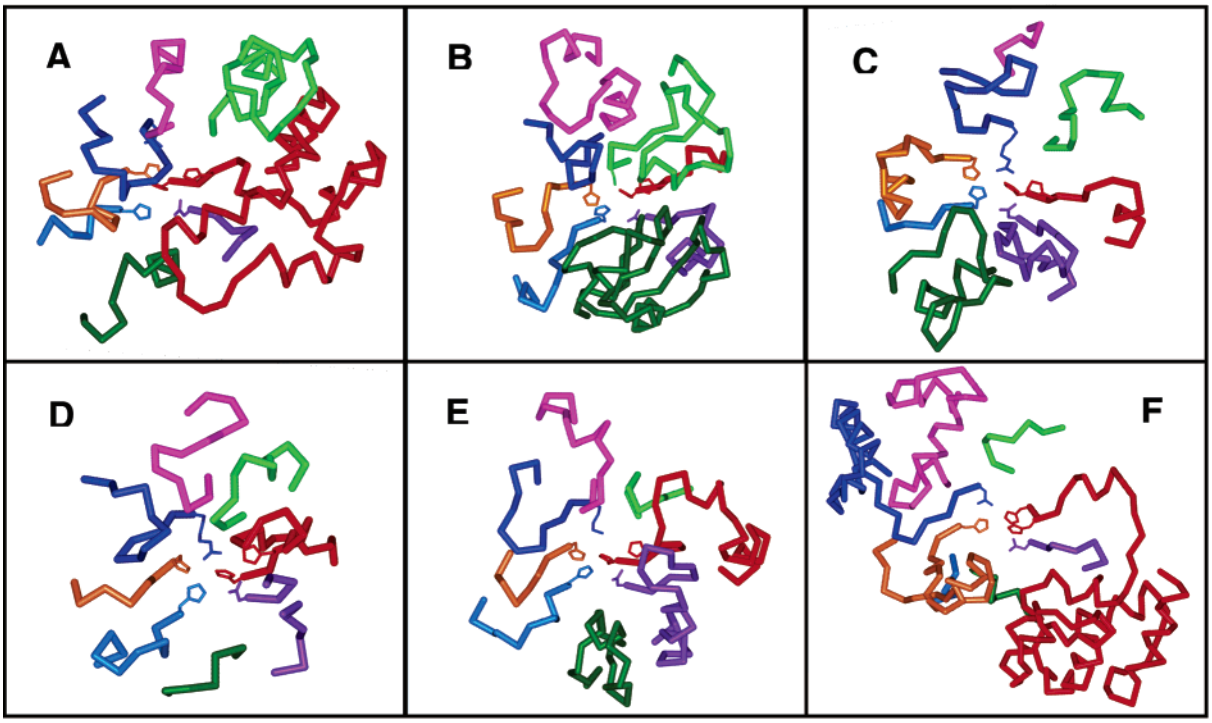

FIGURE 5: The conformational diversity among the loops that follow the eight β-strands within the β-barrels the amidohydrolases. The loop colors are coded as 1, red; 2, purple; 3, dark green; 4, bright blue; 5, orange; 6, dark blue; 7, pink; and 8, bright green. The identity of the enzymes are ADA, from PDB file: 1a4m (A); DAA, from PDB file: 1m7j (B); DHO, from PDB file: 1j79 (C); IAD, from PDB file: 1onw (D); PTE, from PDB file: 1hzy (E); and URI, from PDB file: 1j5s (F).

are used to create the superpositions. The positional conservation of the metal ligands to one another may reflect the high evolutionary barrier that would have to be overcome to simultaneously rearrange the positions of the metal ligands.

LOOPS AND ACTIVE SITES

In a manner reminiscent of the hypervariable regions in antibodies, the eight loops that are found immediately after the residues that bind the divalent cations vary immensely in sequence, length, and conformation despite the strong structural conservation of the preceding β-strands and the α-helices that follow. The conformational diversity of the loops, starting with the residues immediately following the end of the β-strands and ending in a common region at or near the N-termini of the α-helices is shown in Figure 5. All of these loops show substantial variability in length. Uronate isomerase has several loops (1, 3, and 4) that are much longer than the typical loops found in the other structures (*3*). Loop 1 of URI comprises 102 residues and contains six helices that form a distinct subdomain. The first loops of both ADA (*16*) and CDA (*17*) are also somewhat large (72 residues forming four helices and 47 residues forming two helices, respectively). The loops do not fold back on the active site to contact substrates, products, or inhibitors. In the structurally characterized members of the amidohydrolase superfamily only 18 of the 64 loops contact the substrate, product, or inhibitor in the structures that contain small molecules bound within the active site. In general, loops 7 and 8 are most often involved in contacting the ligands in the active site.

Access to the active sites in some of these enzymes requires conformational changes. For example, both ADA and CDA have relatively large substrates but small channels for entry into their active sites. Loop 1 has direct contact with substrate analogues in both ADA and CDA. In ADA it appears that Trp-117 or the mobile loop after strand 2 containing Trp-117 acts as a gatekeeper for entry into the active site. The restricted access to the active site suggests that the catalytic interconversion between substrate and product is sequestered from the bulk solvent. In IAD, loops 1−4 have direct contact with the product, aspartate. In addition, the binding site for IAD appears to be accessible only from the side and not from the top as viewed from the β-barrel, unlike most of the other proteins (*9*). However, in the absence of aspartate, the residues covering the active site are highly mobile and probably do not block the entry of dipeptides. The temperature factors for the loop that covers the active site are very high, even in the presence of the product, aspartate. In the crystal structure of DHO the product, dihydroorotate, is found bound to one subunit, while the substrate, carbamoyl aspartate, is bound to the adjacent subunit within the same dimeric complex (*8*). The biggest difference in the conformational geometry between the two subunits is found in loop 4. The changes in the orientation of loop 4 may mediate the catalytic interconversion between substrate and product in this enzyme. The positioning of a substrate analogue at the top of the β-barrel in PTE is presented in Figure 6.

Many of the proteins make contact with the substrates through loops 6, 7, and 8. In RDP, loop 6 makes contact with a substrate analogue (*13*). Loop 7 has contact with bound small molecule ligands in PTE, URE (*Bacillus pasteurii*), DHO and RDP. Loop 8 interacts with substrate analogues in PTE, URE (*B. pasteurii*), CDA, IAD, and RDP. There is a large change in the position of loop 7 in URE (*B. pasteurii*) when inhibitor is bound. The binding site for DAA

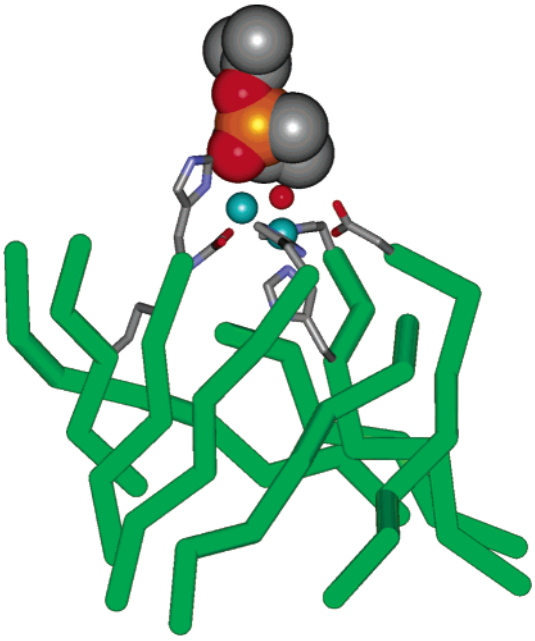

FIGURE 6: Orientation of a substrate analogue directly above the binuclear metal center of PTE. The eight β-strands are shown in bright green (from PDB file: 1ez2). The two metal ions are shown as blue spheres and the metal ligands are illustrated in a stick format.

appears to be collapsed in the crystal structure (*15*). There is, however, a very narrow bent channel that leads from the bulk solvent into the active site. The loops in this region have a slight elevation in the temperature factors, and their mobility may enable the substrate to enter the active site. Sequestering the substrates from bulk solvent may be important for DAA. In contrast, RDP does not appear to sequester the substrate from solvent. The structures for wild-type variants of HYD that are stereoselective for the hydrolysis of hydantoins of amino acids have been determined (*10*−*12*). A proposal has been made for how the orientation of substrates within the active sites leads to a discrimination between enantiomers (*11*, *12*).

For all of these enzymes, the primary active site architecture is one that has evolved for the production and delivery of hydroxide to an acceptor substrate. The structural motifs for the activation of the hydrolytic water molecule are largely conserved, while the part of the active site that is contributed by the loops to define the substrate specificity shows substantial variability.

MECHANISMS OF ACTION

The elements of the catalytic reaction mechanisms have been examined in detail for some members of the amidohydrolase superfamily. The best documented case is that catalyzed by dihydroorotase from *E. coli* (*8*, *24*). With DHO the crystal structure was solved in the presence of carbamoyl aspartate at a pH where the thermodynamic equilibrium constant between dihydroorotate and carbamoyl aspartate is near unity (*8*). DHO is a dimer and the crystal structure shows that the substrate and product are bound to separate monomeric units within the dimeric protein. Therefore, this structure revealed the specific interactions within the active site immediately before and after the enzymatic reaction had occurred. In the case of dihydroorotate, the carbonyl group of the amide bond about to be cleaved is found interacting

Scheme 2

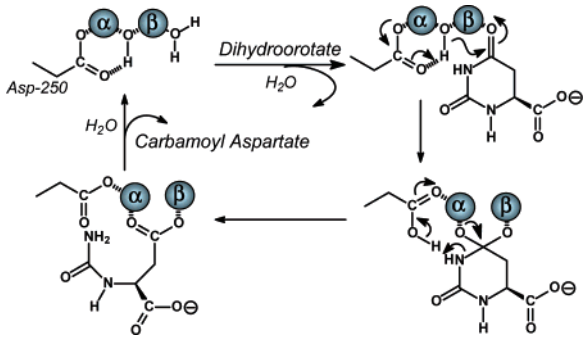

with the β-metal ion. This interaction serves to polarize the amide bond and make the carbonyl carbon more electrophilic. The bridging hydroxide is poised for nucleophilic attack at the *re*-face of the carbonyl group. In addition, the aspartate from strand 8 is hydrogen bonded to the bridging hydroxide and is positioned to function as a proton shuttle between substrate and product. In the enzyme complex with carbamoyl aspartate the newly formed carboxylate group is found as a bridge between the two divalent cations. This result demonstrates that the water of hydrolysis originated with the bridging hydroxide. During the cleavage of dihydroorotate the nitrogen of the amide bond must be protonated. The only residue that is positioned in a manner that can serve this function is the carboxylate from the invariant aspartate from strand 8. A mechanism that is consistent with the structural and biochemical information is presented in Scheme 2 (*8*, *25*). Mechanisms that are entirely analogous to the one presented in Scheme 2 for DHO have also been proposed for PTE and IAD (*24*, *9*). However, somewhat different mechanisms have been proposed for URE (*26*, *27*). Benini et al. have argued for the polarization of the carbonyl group by coordination with M_β and complexation of M_α by one of the two amide nitrogens of the substrate (*26*). Proton transfer to the leaving group is facilitated by the bridging hydroxide and a hydrogen bonding interaction from a conserved histidine that originates from the loop that follows strand 7. In a competing mechanism proposed by Hausinger and coworkers, proton transfer to the leaving group originates directly from a histidine from loop 7 rather than the aspartate from strand 8 (*27*).

The reaction mechanism for the elimination of ammonia in adenosine deaminase has also received significant interrogation (*16*, *20*). Adenosine deaminase has a subtype III mononuclear metal center and the enzymatic reaction is an example of a nucleophilic aromatic substitution by water. In the subtype III metal centers, the lone metal ion is positioned in the M_α position. In these mononuclear examples the histidine from strand 5 coordinates the lone metal ion in addition to the two histidines from strand 1 and the invariant aspartate from strand 8. The histidine from strand 6 apparently functions as a general base in the abstraction of a proton from the water molecule bound to the metal center. The incipient hydroxide attacks the aromatic ring to form a tetrahedral intermediate. This reaction is activated by proton donation from a glutamate that is found three residue positions beyond the conserved histidine from strand 5. This HxxE motif at the end of stand 5 is found in every one of the known amidohydrolase enzymes that catalyze a nucleophilic aromatic substitution reaction except for adenine

Scheme 3

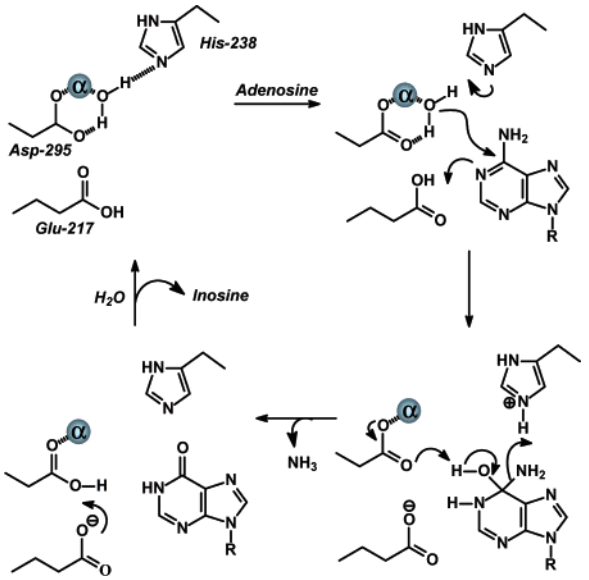

deaminase. These examples include adenosine deaminase (*16*), AMP deaminase (gi: 608497), guanine deaminase (gi: 16130785), cytosine deaminase (*17*), and the proteins annotated as chlorohydrolases (*28*, PDB entry 1j6p). Collapse of the tetrahedral intermediate is facilitated by proton donation from the protonated histidine from strand 6 and proton transfer from the carbinol to the aspartate from strand 8 or the glutamate from strand 6, depending on whether the enol or the keto form of inosine is the primary product. A reaction mechanism for adenosine deaminase is presented in Scheme 3.

SUMMARY

The amidohydrolase superfamily comprises a remarkable set of enzymes that catalyze the hydrolysis of a wide range of substrates bearing amide or ester functional groups at carbon and phosphorus centers. In all cases, the nucleophilic water molecule is activated through complexation with a mononuclear or binuclear metal center. Seven variations in the identity of the specific amino acid metal ligands have been structurally characterized by X-ray crystallography. In the binuclear metal centers the carbonyl and phosphoryl groups are polarized through Lewis acid catalysis via complexation with the β-metal ion, while the solvent molecule is activated for nucleophilic attack by interaction with the α-metal ion. In the mononuclear metal centers, the substrate is activated by proton transfer from the active site, and the water is activated by metal ligation and general base catalysis. The metal centers are perched at the C-terminal end of the β-barrel core within a $(\beta\alpha)_8$ structural domain. The substrate diversity is dictated by the conformational restrictions imposed by the eight loops that extend from the ends of the eight β-strands.

ACKNOWLEDGMENT

We thank Professors Hazel M. Holden (Wisconsin), Patricia Babbitt (UCSF), and John A. Gerlt (Illinois) for many insightful discussions concerning the structure and function of the amidohydrolase superfamily.

REFERENCES

1. Holm, L., and Sander, C. (1997) An Evolutionary Treasure: Unification of a Broad Set of Amidohydrolases Related to Urease, *Proteins: Struct., Funct., Genet. 28*, 72−82.
2. Buchbinder, J. L., Stephenson, R. C., Dresser, M. J., Pitera, J. W., Scanlan, T. S., and Fletterick, R. J. (1998) Biochemical Characterization and Crystallographic Structure of an *Escherichia coli* Protein from the Phosphotriesterase Gene Family, *Biochemistry 37*, 5096−5106.
3. Schwarzenbacher, R., Canaves, J. M., Brinen, L. S., Dai, X., Deacon, A. M., Elsliger, M. A., Eshaghi, S., Floyd, R., Godzik, A., Grittini, C., Grzechnik, S. K., Guda, C., Jaroszewski, L., Karlak, C., Klock, H. E., Koesema, E., Kovarik, J. S., Kreusch, A., Kuhn, P., Lesley, S. A., McMullan, D., McPhillips, T. M., Miller, M. A., Morse, A., Moy, K., Ouyang, J., Robb, A., Rodrigues, K., Selby, T. L., Spraggon, G., Stevens, R. C., van den Bedem, H., Velasquez, J., Vincent, J., Wang, X., West, B., Wolf, G., Hodgson, K., Wooley, J., and Wilson I. A. (2003) Crystal Structure of Uronate Isomerase (Tm0064) from *Thermotoga maritima* at 2.85 Å Resolution, *Proteins: Struct., Funct., Genet. 53*, 142−145.
4. Benning, M. M., Shim, H., Raushel, F. M., and Holden, H. M. (2001) High-Resolution X-ray Structures of Different Metal-Substituted Forms of Phosphotriesterase from *Pseudomonas diminuta*, *Biochemistry 40*, 2712−2722.
5. Benning, M. M., Hong, S.-B, Raushel, F. M., and Holden, H. M. (2000) The Binding of Substrate Analogs to Phosphotriesterase, *J. Biol. Chem. 275*, 30556−30560.
6. Benini, S., Rypniewski, W. R., Wilson, K. S., Miletti, S., Ciurli, S., and Mangani, S. (1999) A New Proposal for Urease Mechanism Based on the Crystal Structures of the Native and Inhibited Enzyme from *Bacillus pasteurii*: Why Urea Hydrolysis Costs Two Nickels, *Struct. Folding Des. 7*, 205−216.
7. Jabri, E., Carr, M. B., Hausinger, R. P., and Karplus, P. A. (1995) The Crystal Structure of Urease from *Klebsiella aerogenes*, *Science* 268, 998−1004.
8. Thoden, J. B., Phillips, G. N., Jr., Neal, T. M., Raushel, F. M., and Holden, H. M. (2001) Molecular Structure of Dihydroorotase: A Paradigm for Catalysis Through the Use of a Binuclear Metal Center, *Biochemistry 40*, 6989−6997.
9. Thoden, J. B., Marti-Arbona, R., Raushel, F. M., and Holden, H. M. (2003) High-Resolution X-ray Structure of Isoaspartyl Dipeptidase from *Escherichia coli*, *Biochemistry 42*, 4874−4882.
10. Abendroth, J., Niefind, K., and Schomburg, D. (2002) X-ray Structure of a Dihydropyrimidinase from *Thermus* Sp. at 1.3 Å Resolution, *J. Mol. Biol. 320*, 143−156.
11. Cheon, Y. H., Kim, H. S., Han, K. H., Abendroth, J., Niefind, K., Schomburg, D., Wang, J., and Kim, Y. (2002) Crystal Structure of D-Hydantoinase from *Bacillus stearothermophilus*: Insight into the Stereochemistry of Enantioselectivity, *Biochemistry 41*, 9410−9417.
12. Abendroth, J., Niefind, K., May, O., Siemann, M., Syldatk, C., and Schomburg, D. (2002) The Structure of L-Hydantionase from *Arthrobacter aurescens* Leads to an Understanding of Dihydropyrimidinase Substrate and Enantio Specificity, *Biochemistry 41*, 8589−8597.
13. Nitanai, Y., Satow, Y., Adachi, H., and Tsujimoto, M. (2002) Crystal Structure of Human Renal Dipeptidase Involved in Beta-Lactam Hydrolysis, *J. Mol. Biol. 321*, 177−184.
14. Vincent, F., Yates, D., Garman, E., Davies, G. J., and Brannigan, J. A. (2004) The Three-Dimensional Structure of the N−Acetylglucosamine-6-Phosphate Deacetylase, NagA, from *Bacillus subtilis*: A Member of the Urease Superfamily, *J. Biol. Chem. 279*, 2809−2816.
15. Liaw, S.-H., Chen, S.-J., Ko, T.-P., Hsu, C.-S., Chen, C. J., Wang, A. H., and Tsai, Y.-C. (2003) Crystal Structure of D-Aminoacylase from *Alcaligenes faecalis* Da1. A Novel Subset of Amidohydrolases and Insights into the Enzyme Mechanism, *J. Biol. Chem. 278*, 4957−4962.
16. Wang, Z., and Quiocho, F. A. (1998) Complexes of Adenosine Deaminase with Two Potent Inhibitors: X-ray Structures in Four Independent Molecules at pH of Maximum Activity, *Biochemistry 37*, 8314−8324.
17. Ireton, G. C., McDermott, G., Black, M. E., and Stoddard, B. L. (2002) The Structure of *Escherichia coli* Cytosine Deaminase, *J. Mol. Biol. 315*, 687−697.

18. Shim, H., and Raushel, F. M. (2000) Self-Assembly of the Binuclear Metal Center of Phosphotriesterase, *Biochemistry 39*, 7357−7364.
19. Mulrooney, S. B., and Hausinger, R. P. (1990) Sequence of the *Klebsiella aerogenes* Urease Genes and Evidence for Accessory Proteins Facilitating Nickel Incorporation, *J. Bacteriol. 172*, 5837−5849.
20. Wilson, D. K., Rudolph, F. B., and Quiocho, F. A. (1991) Atomic Structure of Adenosine Deaminase Complexed with a Transition State Analog: Understanding Catalysis and Immunodeficiency Mutations, *Science 252*, 1278−1284.
21. Porter, D. J., and Austin, E. A. (1993). Cytosine Deaminase: The Roles of Divalent Metal Ions in Catalysis, *J. Biol. Chem. 268*, 24005−24011.
22. Lai W. L., Chou, L. Y., Ting, C. Y., Kirby, R., Tsai, Y. C., Wang, A. H. J., and Liaw, S. H. (2004), The Functional Role of the Binuclear Metal Center in D-Aminoacylase − One-Metal Activation and Second-Metal Attenuation,*J. Biol. Chem. 279*, 13962−13967.
23. Benning, M. M., Kuo, J. M., Raushel, F. M., and Holden, H. M. (1994) The Three-Dimensional Structure of Phosphotriesterase: An Enzyme Capable of Detoxifying Organophosphorus Nerve Agents, *Biochemistry 33*, 15001−15007.
24. Aubert, S. D., Li, Y., and Raushel, F. M. (2004) Mechanism for the Hydrolysis of Organophosphates by the Bacterial Phosphotriesterase, *Biochemistry 43*, 5707−5715.
25. Porter, T. N., Li, Y., and Raushel, F. M. (2004) Mechanism for the Dihydroorotase Reaction, *Biochemistry 43*, 16285−16292.
26. Benini, S, Rypniewski, W. R., Wilson, K. S., and Ciurli, S. (2001) Structure-based Rationalization of Urease Inhibition by Phosphate: Novel Insights into the Enzyme Mechanism, *J. Biol. Inorg. Chem. 6*, 778−790.
27. Pearson M. A., Park, I. S., Schaller, R. A., Michel, L. O., Karplus, P. A., and Hausinger, R. P. (2000) Kinetic and Structural characterization of urease Active Site Variants, *Biochemistry 39*, 8575−8584.
28. Seffernick, J. L., and Wackett, L. P. (2001) Rapid Evolution of Bacterial Catabolic Enzymes: A Case Study with Atrazine Chlorohydrolase, *Biochemistry 40*, 12747−12753.

BI047326V